8. D. J. Willshaw, O. P. Buneman, H. C. Longuet-Higgins, *Nature* **222**, 960–962 (1969).
9. D. Marr, *Philos. Trans. R. Soc. Lond. B Biol. Sci.* **262**, 23–81 (1971).
10. G. Palm, *Biol. Cybern.* **36**, 19–31 (1980).
11. J. J. Hopfield, *Proc. Natl. Acad. Sci. U.S.A.* **79**, 2554–2558 (1982).
12. H. Sompolinsky, *Phys. Rev. A Gen. Phys.* **34**, 2571–2574 (1986).
13. D. J. Amit, H. Gutfreund, H. Sompolinsky, *Phys. Rev. A* **35**, 2293–2303 (1987).
14. M. R. Bennett, W. G. Gibson, J. Robinson, *Philos. Trans. R. Soc. Lond. B Biol. Sci.* **343**, 167–187 (1994).
15. R. Miles, R. K. S. Wong, *J. Physiol.* **373**, 397–418 (1986).
16. R. D. Traub, R. Miles, *Neuronal Networks of the Hippocampus.* (Cambridge Univ. Press, Cambridge, 1991).
17. R. Perin, T. K. Berger, H. Markram, *Proc. Natl. Acad. Sci. U.S.A.* **108**, 5419–5424 (2011).
18. S. Song, P. J. Sjöström, M. Reigl, S. Nelson, D. B. Chklovskii, *PLOS Biol.* **3**, e68 (2005).
19. S. Rieubland, A. Roth, M. Häusser, *Neuron* **81**, 913–929 (2014).
20. D. J. Watts, S. H. Strogatz, *Nature* **393**, 440–442 (1998).
21. J. Lübke, H. Markram, M. Frotscher, B. Sakmann, *J. Neurosci.* **16**, 3209–3218 (1996).
22. H. Markram, J. Lübke, M. Frotscher, A. Roth, B. Sakmann, *J. Physiol.* **500**, 409–440 (1997).
23. T. Branco, K. Staras, *Nat. Rev. Neurosci.* **10**, 373–383 (2009).
24. A. I. Gulyás *et al.*, *Nature* **366**, 683–687 (1993).
25. N. Holderith *et al.*, *Nat. Neurosci.* **15**, 988–997 (2012).
26. R. A. Silver, J. Lübke, B. Sakmann, D. Feldmeyer, *Science* **302**, 1981–1984 (2003).
27. N. Spruston, P. Jonas, B. Sakmann, *J. Physiol.* **482**, 325–352 (1995).
28. Z. Nusser *et al.*, *Neuron* **21**, 545–559 (1998).
29. J. Kowalski, J. Gan, P. Jonas, A. J. Pernía-Andrade, *Hippocampus* **26**, 668–682 (2016).
30. S. Cash, R. Yuste, *Neuron* **22**, 383–394 (1999).
31. S. Kim, S. J. Guzman, H. Hu, P. Jonas, *Nat. Neurosci.* **15**, 600–606 (2012).
32. D. G. Amaral, N. Ishizuka, B. Claiborne, *Prog. Brain Res.* **83**, 1–11 (1990).
33. R. K. Mishra, S. Kim, S. J. Guzman, P. Jonas, *Nat. Commun.* **7**, 11552 (2016).
34. L. Zhao, B. Beverlin 2nd, T. Netoff, D. Q. Nykamp, *Front. Comput. Neurosci.* **5**, 28 (2011).
35. X. G. Li, P. Somogyi, A. Ylinen, G. Buzsáki, *J. Comp. Neurol.* **339**, 181–208 (1994).
36. M. P. Witter, *Learn. Mem.* **14**, 705–713 (2007).
37. E. T. Rolls, *Front. Syst. Neurosci.* **7**, 74 (2013).
38. S. Lefort, C. Tomm, J. C. Floyd Sarria, C. C. Petersen, *Neuron* **61**, 301–316 (2009).
39. N. Brunel, *Nat. Neurosci.* **19**, 749–755 (2016).
40. Y. Deguchi, F. Donato, I. Galimberti, E. Cabuy, P. Caroni, *Nat. Neurosci.* **14**, 495–504 (2011).
41. Y. C. Yu, R. S. Bultje, X. Wang, S. H. Shi, *Nature* **458**, 501–504 (2009).
42. F. Engert, T. Bonhoeffer, *Nature* **399**, 66–70 (1999).
43. D. A. Henze, L. Wittner, G. Buzsáki, *Nat. Neurosci.* **5**, 790–795 (2002).
44. N. P. Vyleta, P. Jonas, *Science* **343**, 665–670 (2014).
45. A. Mitra, S. S. Mitra, R. W. Tsien, *Nat. Neurosci.* **15**, 250–257 (2011).
46. J. E. Hanson, M. Blank, R. A. Valenzuela, C. C. Garner, D. V. Madison, *J. Physiol.* **579**, 53–67 (2007).
47. J. J. Couey *et al.*, *Nat. Neurosci.* **16**, 318–324 (2013).



## ACKNOWLEDGMENTS

We thank A. Aertsen, J. Csicsvari, A. Roth, C. Savin, R. Shigemoto, and two anonymous reviewers for critically reading the manuscript, as well as J. Szabadics and S. Rotter for useful discussions. We are grateful to F. Marr for excellent technical assistance, B. Joch for help with morphological analysis, E. Kramberger for manuscript editing, T. Asenov (Miba machine shop) for technical support, and M. Schunn (preclinical facility) for animal maintenance. We also thank the scientific computing facilities, University of Innsbruck, for help with the MACH computer cluster. Finally, we thank D. Nykamp for providing programs and G. Buzsáki, L. Wittner, G. Ascoli, and D. Ropireddy for sharing CA3 pyramidal neuron models. Supported by the Fond zur Förderung der Wissenschaftlichen Forschung (P 24909-B24 to P.J.), the European Union (European Research Council Advanced Grant 268548 to P.J.), and the Deutsche Forschungsgemeinschaft (FR 620/14-1 to M.F.). M.F. is Senior Research Professor of the Hertie Foundation. The authors declare no conflicts of interest. Original data and programs were stored in the scientific repository of the Institute of Science and Technology Austria and are available on request.

## SUPPLEMENTARY MATERIALS

www.sciencemag.org/content/353/6304/1117/suppl/DC1
Materials and Methods
Figs. S1 to S11
Tables S1 to S4
References (*48*–*68*)

3 January 2016; accepted 15 July 2016
10.1126/science.aaf1836


INHIBITORY SYNAPSES

# Identification of an elaborate complex mediating postsynaptic inhibition


**Akiyoshi Uezu,[1] Daniel J. Kanak,[1]* Tyler W. A. Bradshaw,[1]* Erik J. Soderblom,[1,2] Christina M. Catavero,[1] Alain C. Burette,[3,4] Richard J. Weinberg,[3,4] Scott H. Soderling[1,5]†**



**Inhibitory synapses dampen neuronal activity through postsynaptic hyperpolarization. The composition of the inhibitory postsynapse and the mechanistic basis of its regulation, however, remain poorly understood. We used an in vivo chemico-genetic proximity-labeling approach to discover inhibitory postsynaptic proteins. Quantitative mass spectrometry not only recapitulated known inhibitory postsynaptic proteins but also revealed a large network of new proteins, many of which are either implicated in neurodevelopmental disorders or are of unknown function. Clustered regularly interspaced short palindromic repeats (CRISPR) depletion of one of these previously uncharacterized proteins, InSyn1, led to decreased postsynaptic inhibitory sites, reduced the frequency of miniature inhibitory currents, and increased excitability in the hippocampus. Our findings uncover a rich and functionally diverse assemblage of previously unknown proteins that regulate postsynaptic inhibition and might contribute to developmental brain disorders.**


Two anatomically distinct classes of synapses are present in the central nervous system: excitatory synapses, predominantly localized to postsynaptic spines, and inhibitory synapses, in which the postsynapse is typically embedded in the soma and dendritic shaft (*1*). Purification and analysis of the protein complexes of the excitatory postsynapse have led to fundamental insights in neurobiology. These insights include how receptor trafficking, synaptic adhesion, cytoskeletal remodeling, and protein phosphorylation contribute to the synaptic plasticity underlying learning and memory (*2*, *3*). Moreover, genetic perturbations of excitatory postsynaptic proteins are strongly implicated in developmental brain disorders and psychiatric conditions (*4*, *5*).

In contrast, the biochemical purification and analysis of the inhibitory postsynaptic density (iPSD) has remained largely intractable. Accordingly, the molecular basis of postsynaptic inhibitory synapse regulation and its contribution to neurodevelopmental disorders is poorly understood. Recently, an affinity purification approach, BioID, has been developed that utilizes a promiscuous *Escherichia coli* biotinylation enzyme $BirA^{R118G}$ (here termed BirA, with Gly replacing $Arg^{118}$) fused to a bait protein expressed in cells (*6*). BirA-dependent covalent biotinylation occurs within 10 to 50 nm of the bait protein and allows for efficient isolation and analysis of proximal proteins by streptavidin-based affinity purification and mass spectrometry (MS) (*7*). Compared with affinity purification methods, the BioID reaction is executed in situ and thus enables the capture of protein complexes, including transient interactions and insoluble proteins from subcellular compartments refractory to biochemical isolation (*8*).

We adapted the proximity-dependent biotin identification (BioID) approach to enable in vivo BioID (iBioID) of synaptic complexes in mouse brain. We virally expressed inhibitory or excitatory PSD proteins fused to BirA to capture and purify their associated proteins. The method labels the corresponding postsynaptic structures in vivo, and that enabled the identification of virtually all of the known proteins of the iPSD. It also revealed a large number of previously unknown proteins, including a rich diversity of transmembrane and signaling proteins. These results provide a molecular prospectus for the deeper understanding of synaptic physiology that was, until now, largely confined to the excitatory PSD.

## In vivo capture of synaptic protein complexes

Gephyrin is the major scaffolding protein organizing the iPSD structure, interacting directly with


[1]The Department of Cell Biology, Duke University Medical School, Durham, NC 27703, USA. [2]Duke Proteomics and Metabolomics Shared Resource and Duke Center for Genomic and Computational Biology, Duke University Medical School, Durham, NC 27703, USA. [3]Department of Cell Biology and Physiology, University of North Carolina, Chapel Hill, NC 27599, USA. [4]Neuroscience Center, University of North Carolina, Chapel Hill, NC 27599, USA. [5]The Department of Neurobiology, Duke University Medical School, Durham, NC 27703, USA.
*These authors contributed equally to this work. †Corresponding author: Email: scott.soderling@duke.edu

glycine receptors (GlyRs) or γ-aminobutyric acid type A receptors ($GABA_A$Rs) and other molecules such as neuroligin-2 (NL2) and collybistin (Arhgef9) (*9*–*11*). To label proteins associated with synaptic proteins in the context of native tissue in vivo, we created adeno-associated viral (AAV) constructs for the expression of gephyrin- and the membrane-associated guanylate kinase, PSD protein 95 (PSD-95), fused with BirA, targeting the proteomes of inhibitory and excitatory postsynapses, respectively (Fig. 1A). To control for synapse specificity of biotinylation, we also expressed soluble BirA, which nonspecifically biotinylates proteins throughout the neuron. Each construct was validated by immunocytochemistry to determine its localization and synaptic site of biotinylation (Fig. 1B). To label synaptic structures in vivo, we developed a protocol that maximizes the number of synapses labeled by injection of AAV into the cortex of postnatal day 0 (P0) mouse pups, followed by 7 days of daily doses of exogenous biotin (Fig. 1C). Immunohistochemical analysis validates the approach for in vivo biotinylation (Fig. 1D), which yields punctate labeling of synaptic sites in brain tissue (Fig. 1E). Immuno–electron microscopy verified that biotinylation occurred at symmetric (i.e., inhibitory) synapses for BirA-gephyrin, and at asymmetric (i.e., excitatory) postsynaptic sites for PSD-95–BirA (Fig. 1, F and G). Subcellular sites of background staining (perhaps due to overexpression or detection of endogenous biotinylated carboxylases) were also noted to guide the final proteomic analysis (fig. S1A and table S1). Purification of biotinylated proteins from neurons expressing each BirA fusion protein and subsequent immunoblotting for known components of inhibitory (collybistin) and excitatory (NR2B and GluA1) synapses verified that each bait specifically labeled components of these synaptic sites, versus the nonspecific labeling of our negative control, soluble BirA (Fig. 1H).

## Discovery of the inhibitory postsynaptic proteome

To pilot the identification of proteins labeled by iBioID, we prepared four cohorts each for BirA, PSD-95–BirA, and BirA-gephyrin using the labeling protocol outlined in Fig. 1C. Biotinylated proteins purified by streptavidin affinity purification were identified by liquid chromatography–tandem mass spectrometry (LC-MS/MS). In total, 928 unique proteins were identified from 12 separate LC-MS/MS runs, with unique compliments of proteins enriched over BirA in each synaptic fraction (fig. S1, B to E, and table S2). Analysis of the gephyrin-BirA fraction confirmed the presence of several proteins reported to reside at the iPSD (*10*, *12*), including Arhgef9/collybistin, VASP family proteins Mena and Evl, and IQSEC3, and two proteins of unknown function, which we termed "inhibitory synaptic proteins 1 and 2" or InSyn1 (UPF0583 protein C15orf59 homolog) and InSyn2 (protein family 196a). This pilot study suggested that, although the BirA-gephyrin is highly specific, increased coverage of the iPSD would be desirable. We therefore expanded the analysis of the iPSD by performing the MS/MS analysis using more sensitive instrumentation and by including additional BirA-fusion proteins to further label the iPSD (collybistin-BirA and InSyn1-BirA) (fig. S1, F and G). InSyn1 was included because functional studies (described below) verified that it was an important component of the iPSD. Quantitative high-resolution LC-MS/MS was then performed for each sample (PSD data set: BirA versus PSD-95;

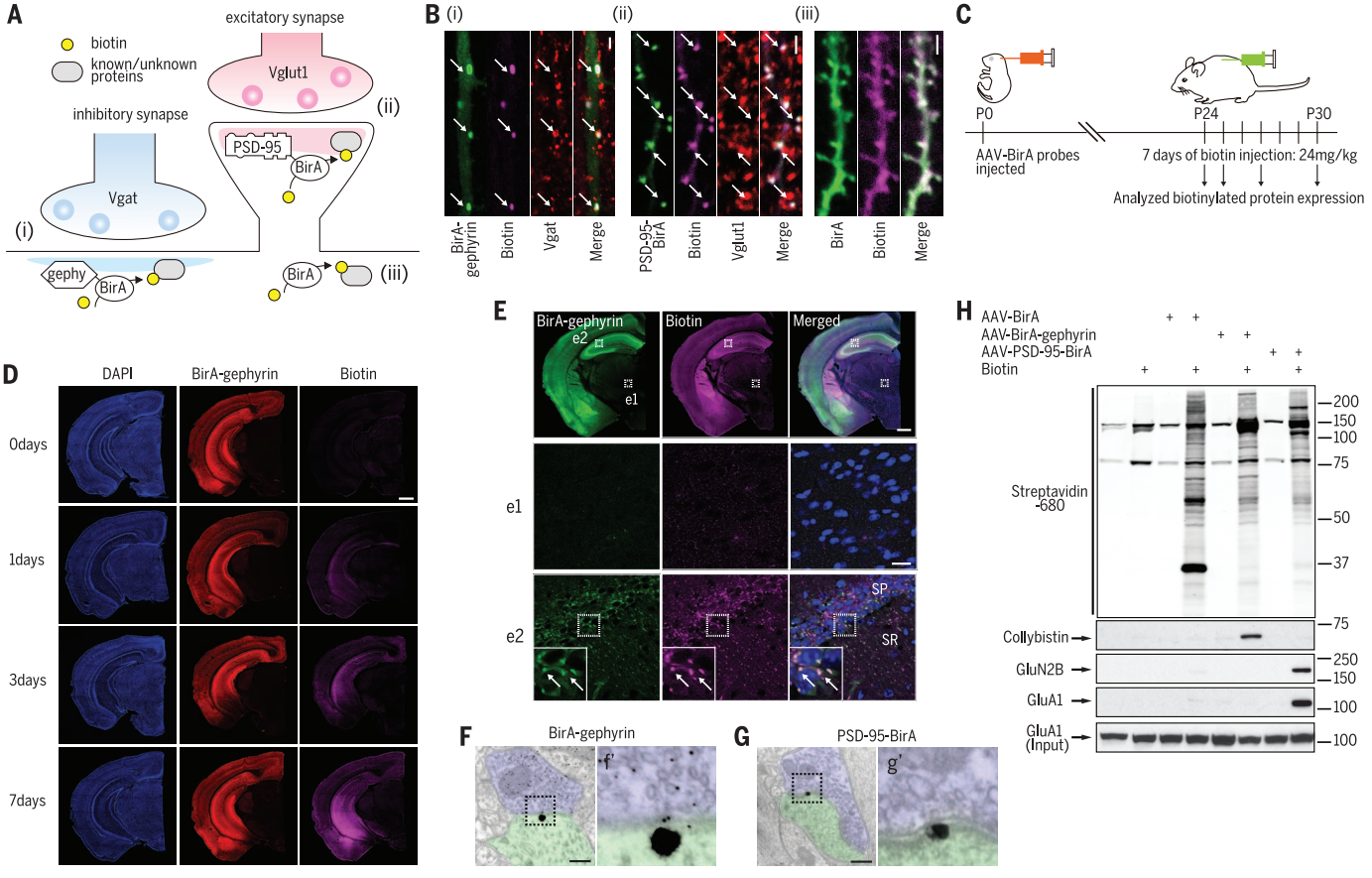


**Fig. 1. Development of iBioID for synaptic proteomics.** (**A**) Schematic of the iBioID approach for synapses. Vglut, vesicular glutamate transporter; Vgat, vesicular GABA transporter. (**B**) Validation of BirA constructs in hippocampal slice using markers labeled in (A): (i) BirA-gephyrin and (ii) PSD-95–BirA (white arrows point to colocalized puncta); and (iii) BirA alone nonspecifically labels proteins. Scale bar, 2 μm. (**C**) Outline of iBioID method in mice. (**D**) Successful biotinylation of proteins in vivo following intraperitoneal biotin administration. Scale bar, 0.5 mm. (**E**) Biotinylation is specific to regions expressing BirA-gephyrin (coronal section). (Insets) From thalamus (e1) and hippocampus (e2) and insets of e2 are shown. Scale bars: top right, 0.5 mm; e1 and e2, 20 μm. Electron micrographs verify enrichment of biotinylation at (**F** and **f'**) inhibitory or (**G** and **g'**) excitatory PSD substructures. Large gold beads, streptavidin labeling; small gold beads, immunolabel for GABA. Scale bar, 250 nm. (**H**) Specific purification of known PSD proteins for each BirA fusion protein.

iPSD data set: BirA versus gephryin, collybistin, InSyn1) in biological triplicates (seven to eight mice per biological fraction). For the excitatory PSD-95 data set, 18,207 peptides corresponding to 2533 unique proteins were quantified, whereas 17,024 peptides corresponding to 2183 proteins were quantified from the iPSD data sets. Proteins were considered enriched in the bait fraction if their average BirA-fusion protein amounts were at least two times the amount of BirA-alone fractions with $P < 0.05$. On the basis of these criteria, 121 excitatory PSD (ePSD) proteins (fig. S2) were specifically labeled by PSD-95–BirA (table S3). More than 95% of the ePSD proteins identified by iBioID were previously known ePSD components, as identified by traditional PSD biochemical fractionation and MS (116 of 121 proteins), demonstrating the specificity of the method. These proteins included glutamate receptors, scaffolding proteins, and signaling proteins of excitatory synaptic complexes. The iPSD data set identified a combined 181 proteins (table S4), including nearly all previously reported proteins of the iPSD (*13*); this data set suggested that coverage of the iPSD had approached saturation (Fig. 2). We also identified a large number of proteins not previously known to reside at the iPSD,

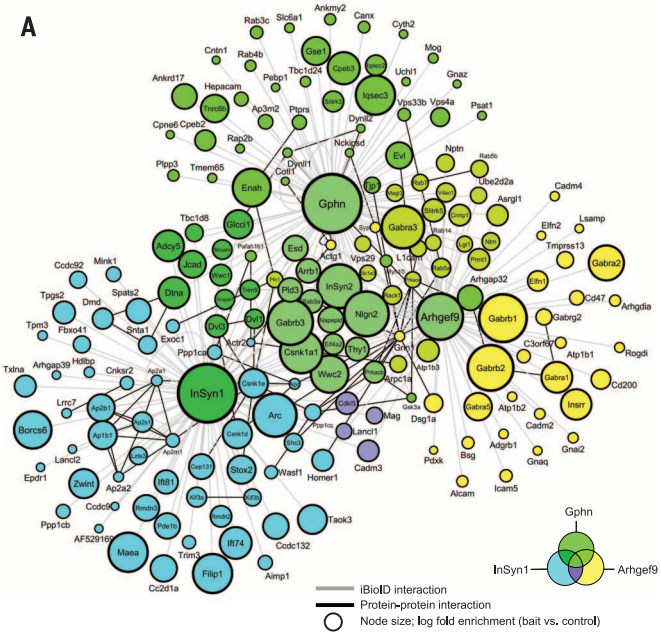


**Fig. 2. Scale-free graph of the iPSD proteome.** (**A**) InSyn1 (blue), gephyrin (green), and arhgef9 (yellow) BirA-dependent iBioID identify a rich network of known and previously unknown proteins enriched at the iPSD. Node titles correspond to gene name; size represents fold-enrichment over negative control. Edges are shaded according to the types of interactions (gray, iBioID; black, protein-protein interactions previously reported). (**B**) Clustergram topology of iPSD proteins (red) in selected functional categories.

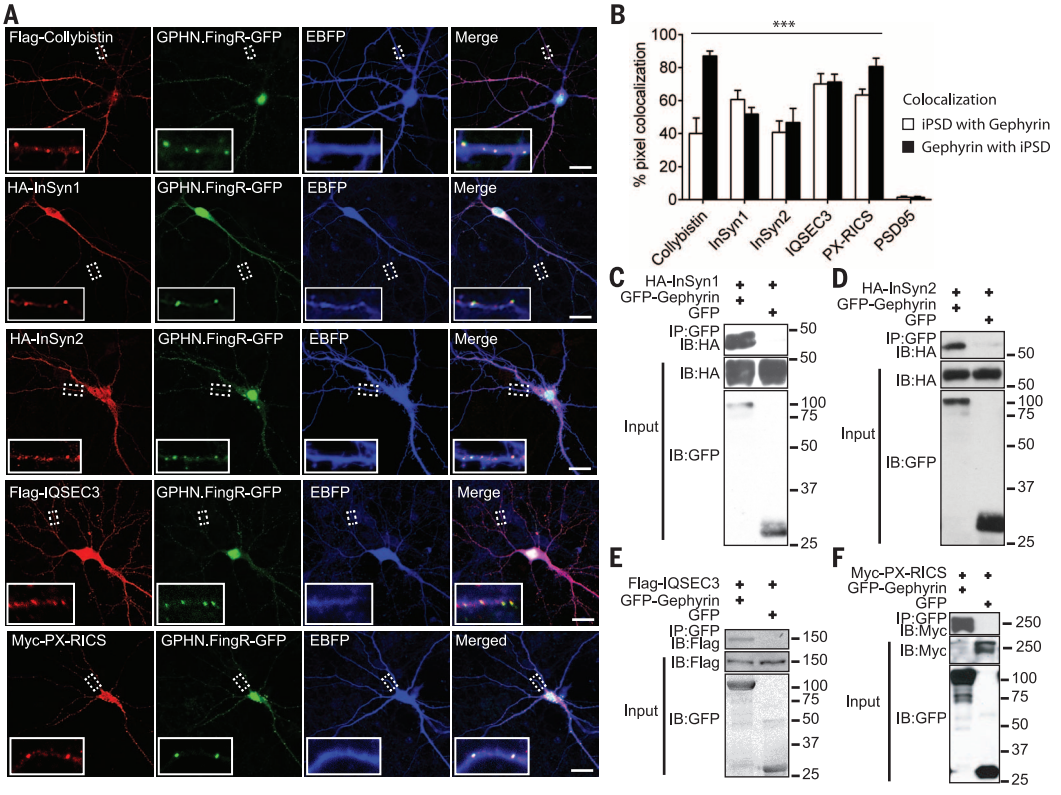


**Fig. 3. Validation of selected iPSD proteins.** (**A**) Colocalization of iPSD proteins (column 1), some Flag-tagged, some hemagglutinin tagged, and Myc–PX-RICS (Myc epitope–tagged Phox domain–containing isoform of RhoGAP involved in β-catenin–*N*-cadherin and *N*-methyl-D-aspartate receptor signaling) with endogenous gephyrin (column 2) in hippocampal neurons. EBFP, enhanced blue fluorescent protein. Scale bar, 10 μm. (**B**) Each iPSD protein significantly colocalizes with gephyrin in dendrites compared with PSD-95 ($n > 9$ dendritic regions of interest). (**C** to **F**) iPSD proteins coimmunoprecipitate with gephyrin when coexpressed in human embryonic kidney 293 (HEK293) cells. ***$P < 0.001$ one-way analysis of variance (ANOVA) followed by Dunnett's multiple comparisons test (B). Error bars ±SEM.

including trafficking proteins, cytoskeletal regulatory proteins, integral membrane proteins, and several protein kinases and phosphatases (Fig. 2B). Many of these proteins (27/181) are encoded by genes implicated in either seizure susceptibility in humans or mice or other brain disorders such as intellectual disability (table S4). Comparison of iPSD and PSD-95 identified 17 proteins shared by the two data sets, 50% of which are signaling proteins (table S5).

### Candidate iPSD proteins colocalize and coimmunoprecipitate with gephyrin

To validate our iBioID results, select iPSD proteins [InSyn1, InSyn2, IQSEC3, collybistin (Arhgeg9), and PX-RICS (Arhgap32)] were cloned and coexpressed in primary neuronal cells with GPHN. FingR-GFP, a recombinant protein sensor of endogenous gephyrin fused to green fluorescent protein (GFP) (*14*) (Fig. 3A). Collybistin served as a positive control, and PSD-95 colocalization served as a negative control. Quantification of colocalizing pixels (Fig. 3B) demonstrated that each iPSD protein extensively overlapped with endogenous gephyrin. Each candidate protein was also tested in coimmunoprecipitation experiments. Epitope-tagged iPSD proteins specifically coprecipitated with GFP-gephyrin, including InSyn1 and InSyn2 (Fig. 3, C to F).

### InSyn1 and InSyn2 are iPSD proteins functionally important for GABAergic inhibition

InSyn1 is a previously uncharacterized protein that lacks protein domains of known function, but whose extensive iBioID interactions with core components of the iPSD (gephyrin, neuroligin-2, collybistin, and $GABA_AR$ subunit β-3) suggested a central role in $GABA_AR$-dependent synaptic inhibition. To test whether InSyn1 is functionally important for synaptic inhibition, we used depletion of the endogenous protein mediated by single-cell clustered regularly interspaced short palindromic repeats (CRISPRs) (*15*) (Fig. 4A). $GABA_AR$-mediated miniature inhibitory postsynaptic currents (mIPSCs) were recorded from CA1 pyramidal cells in hippocampal slices that were biolistically transfected with GFP, spCas9, and validated InSyn1 guide RNA (gRNA) (Fig. 4B). Untransfected (GFP-negative) cells located within a 400-μm radius from GFP-positive cells served as controls, and gRNA specificity was tested by reexpression of Cas9-resistant cDNAs (Fig. 4B). Inhibitory currents were confirmed to be GABAergic because they were reversibly abolished in the presence of bicuculline (1 μM) (fig. S3A). To verify the efficacy of the CRISPR strategy for functional testing of iPSD synaptic proteins, we targeted the obligatory γ2 subunit of the $GABA_AR$ and found a complete abolition of mIPSCs (fig. S3B). We also verified

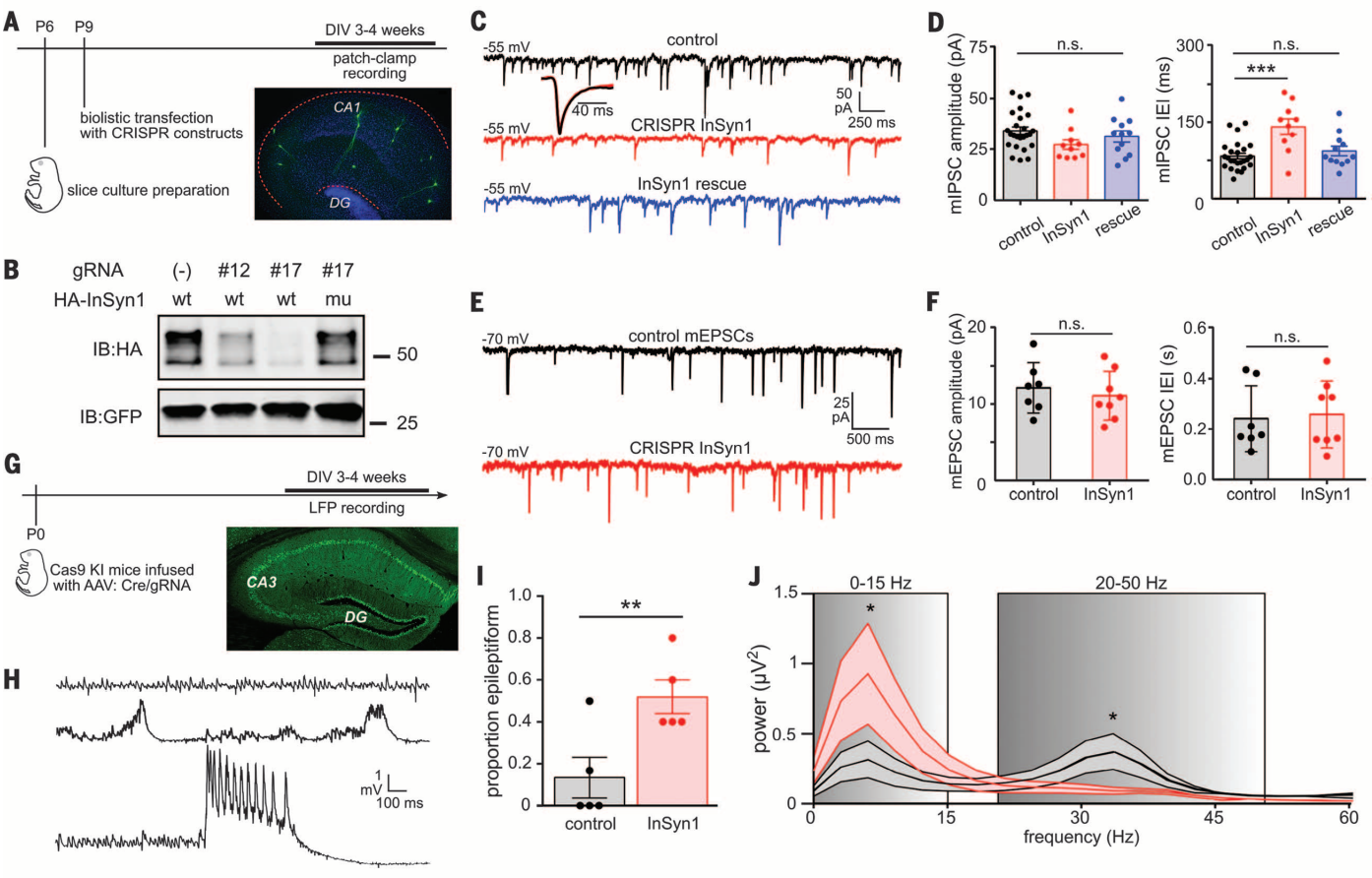


**Fig. 4. Abnormal synaptic inhibition follows loss of the iPSD protein InSyn1.** (**A**) Experimental schematic for (C) to (F). DIV, days in vitro. (**B**) Validation of InSyn1 gRNAs (#12 and #17) and rescue constructs by cotransfection of 293T cells and immunoblotting. (**C** and **D**) $GABA_A$-dependent miniature inhibitory postsynaptic currents ($GABA_A$ mIPSCs) recorded from CA1 pyramidal cells. (Inset) $GABA_A$ mIPSC waveform averages. InSyn1 depletion did not alter mIPSC kinetics (rise: controls, 3.6 ± 0.6 ms; InSyn1, 3.4 ± 0.6 ms; $P = 0.51$; decay: controls, 9.7 ± 2.1 ms; InSyn1, 10.3 ± 1.8 ms; $P = 0.42$). IEIs of InSyn1-depleted $GABA_A$ mIPSCs (red) are specifically increased compared with control (black) and rescue (blue) neurons. (**E** and **F**) AMPAR-dependent mEPSCs are not altered in InSyn1-depleted neurons. (**G**) Time-line schematic for local field potential (LFP) recordings in acute slices from Cas9 knock-in (KI) mice infected with AAV:Cre/Insyn1 gRNA. Representative extent of AAV infection in hippocampus. (**H**) Representative LFP activities recorded in hippocampal area CA3 in the presence of 10 μM carbachol to model "awake state" gamma rhythm. Top trace, Pure 30 to 40 Hz gamma oscillation; middle trace, 3 to 5 Hz spike-wave discharges; bottom trace, ictal-like burst—the latter two indicative of hyperexcitable or epileptiform activity. (**I**) InSyn1 gRNA–expressing slices exhibit increased–epileptiform activity. (**J**) Averaged power spectra showing signal energy in the InSyn1 gRNA-expressing slices is increased in the 0 to 15 Hz frequency band and decreased in the 20 to 50 Hz frequency bands. *$P < 0.05$, **$P < 0.01$; ***$P < 0.001$; n.s., not statistically significant. Error bars ± SEM.

that biolistic transfection of GFP alone did not alter mIPSC characteristics (fig. S3, C to E). Using sgRNA targeting InSyn1 with and without an InSyn1 rescue construct, we found a significant and reversible 69% increase in mIPSC interevent intervals (IEI); the difference in amplitude was not statistically significant (Fig. 4, C and D). The effect of InSyn1 gRNA was specific to inhibitory currents, as α-amino-3-hydroxy-5-methyl-4-isoxazolepropionic

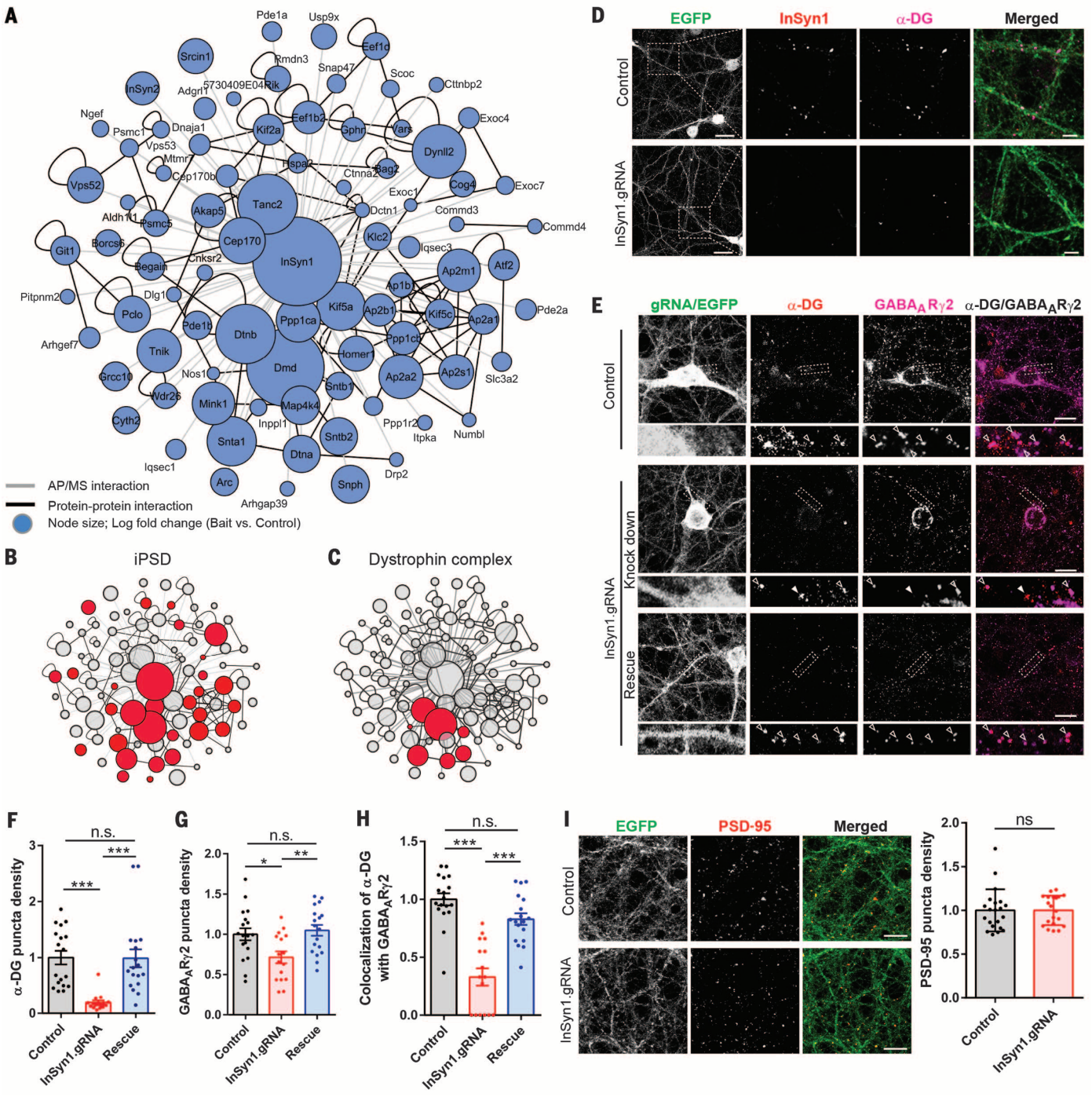


**Fig. 5. InSyn1 functionally associates with the dystrophin complex at the iPSD.** (**A**) Network analysis of affinity-purified InSyn1-GFP proteome from mouse brain. Affinity purification–mass spectrometry (AP/MS) interaction. (**B** and **C**) Clustergram topologies of InSyn1-associated proteins in selected functional categories. (**D**) Colocalization of InSyn1 with α-dystroglycan (α-DG) is diminished after depleting InSyn1 with Cas9 conditional knock-in mouse hippocampal neurons infected with AAV:Cre/Insyn1 gRNA. EGFP, enhanced GFP. Scale bar, 10 μm. (**E**) InSyn1 is essential for $GABA_AR$ and α-DG cluster density. Hippocampal neurons from Cas9 KI mice were stained for $GABA_A$ subunit Rγ2 and α-DG following infection with control AAV:Cre/(-)gRNA (top panel, control); AAV:Cre/Insyn1 gRNA (middle panel, knockdown), or AAV:Cre/Insyn1 gRNA, and transfected with InSyn1 gRNA–resistant plasmid (bottom panels, Rescue). (Insets) Higher magnification regions with open (colocalized puncta) and closed (noncolocalized puncta) arrows. (**F** to **H**) Quantification of α-DG and $GABA_AR\gamma2$ puncta colocalization or density ($n$ = 16 to 18). *$P$ < 0.05, **$P$ < 0.01, ***$P$ < 0.001 one-way ANOVA followed by Tukey's multiple comparisons test (F) to (H). Error bars ± SEM. Scale bar, 10 μm. (**I**) Loss of InSyn1 does not alter PSD-95 puncta density. Cas9 knock-in mouse hippocampal neurons infected with AAV:Cre/Insyn1 gRNA were stained with PSD-95 and quantified ($n$ = 18 to 20 neurons); n.s., not significant, by two-tailed $t$ test (I).

acid receptor (AMPAR)–mediated miniature excitatory postsynaptic current (mEPSC) characteristics were unaltered (Fig. 5, E and F). To further test the predictive value of the iPSD data set, we performed analogous experiments targeting InSyn2. Depletion of InSyn2 resulted in a specific and reversible 62% increase of mIPSC IEI (fig. S4).

Given the large effect of InSyn1 depletion on mIPSC frequency, we next asked whether the inhibitory deficits evident at the single-cell level manifest at the network level. We used a carbachol (CCH)–induced model of the "awake-state" gamma rhythm, which is critically dependent on GABAergic inhibition (*16*). P0 *Rosa26-LSL-Cas9* (*17*) pups were bilaterally infused with AAV:*Cre/InSyn1:gRNA* virus or AAV:*Cre/(-):gRNA* control virus in the hippocampus (Fig. 4G). In the majority of hippocampal slices prepared from control mice and kept vital in vitro, CCH induced a pure gamma rhythm with peak frequencies of ~30 to 40 Hz (Fig. 4H, top trace). In contrast, the majority of InSyn1 gRNA-infected slices exhibited a mixture of gamma oscillations with hyperexcitable events including interictal epileptiform discharges (IEDs) (Fig. 4H, middle trace) and prolonged (2- to 5-s) bursts resembling ictal discharges (Fig. 4H, lower trace). Overall, we found a fourfold increase in the proportion of slices with IEDs (Fig. 4I). Power spectral analysis revealed a 2.2-fold increase in low-frequency (0 to 15 Hz) power corresponding to epileptiform activity, and a 42% reduction in gamma-band (20 to 50 Hz) power (Fig. 4J). These effects likely reflect loss of GABAergic inhibition, as bath application of low concentrations of bicuculline (0.5-μM steps) abolished the gamma rhythm in control slices and induced epileptiform activity similar to that seen in InSyn1 gRNA slices (fig. S3F).

### InSyn1 functions via the dystrophin complex at inhibitory synaptic sites

We next analyzed how InSyn1 functions at inhibitory synapses by further examining its interacting proteins and how its loss alters the iPSD. InSyn1-GFP expressed in hippocampal neurons colocalized with gephyrin in dendritic shafts (fig. S5A). InSyn1-GFP protein or GFP protein alone was virally expressed in the frontal cortex and hippocampus of C57BL/6 mice with AAV and precipitated with GFP-trap resin. InSyn1-GFP and GFP alone coprecipitating proteins were analyzed by LC-MS/MS and compared. InSyn1, pulldown fractions were enriched with 86 proteins (Fig. 5A and table S6) and formed a highly interconnected protein-protein interaction network that included many proteins in the iBioID iPSD (including InSyn2, gephyrin, and Iqsec3) (Fig. 5B).

Among the most enriched proteins were seven components of the dystrophin complex, including dystrophin (DMD), dystrobrevin alpha and beta (Dtna and Dtnb), and alpha-1–, beta-1–, and beta-2–syntrophins (Snta1, Sntb1, and Sntb2) (Fig. 5C). In brain, the dystrophin complex is a component of the iPSD, and its loss in muscular dystrophies contributes to cognitive impairments and epilepsy (*18*). InSyn1-BirA also captured multiple components of the dystrophin complex (Fig. 2, A and B), which suggests that InSyn1-BirA forms a physical complex with both gephyrin and the dystrophin complex. Affinity-purified antibody against InSyn1 (anti-InSyn1) recognized a band of about 50 to 52 kD from cells transfected with hemagglutinin epitope–tagged (HA)–InSyn1 or from mouse brain extract (fig. S5B). Immunofluorescence demonstrated that InSyn1 colocalizes with endogenous α-dystroglycan (α-DG); this punctate staining was lost in neurons cultured from *Rosa26-LSL-Cas9* mice and infected with AAV:Cre/InSyn1:gRNA virus (Fig. 5D). Quantitative analysis demonstrated that InSyn1 gRNA-infected neurons had significant reductions in densities of both α-DG and $GABA_AR$ puncta and a significant reduction in their colocalization (Fig. 5, E to H). In contrast, the density of PSD-95 puncta was unaffected (Fig. 5I). These results are consistent with the reduced mIPSC frequencies we observed in single-neuron CRISPR-mediated InSyn1 depletion and support the notion that the loss of postsynaptic sites of inhibition occurs in the absence of InSyn1.

## Discussion

We report here the in vivo application of the BioID approach to analyze the local proteome of the postsynaptic compartment of inhibitory synapses by quantitative mass spectrometry. Comparing this approach with prior reports of the iPSD using affinity purification (*19*–*21*), iBioID offers important advantages. Nearly all proteins previously reported to exist at the iPSD were identified. iBioID also identified 140 proteins not previously associated with the iPSD, including a wide range of signaling, transmembrane, structural, and uncharacterized proteins. Although we included multiple controls (BirA alone and electron microscopy analysis of nonspecific label) for the overexpression strategy, we anticipate future studies with endogenous proteins fused to BirA will likely further refine the iBioID approach.

To validate our results and to determine how the iPSD is regulated, we focused on two proteins of unknown function, InSyn1 and InSyn2, that associate with several core components of the iPSD. When expressed in neurons, both colocalized with endogenous gephyrin, and their loss resulted in a significant reduction in mIPSC frequency, confirming the validity of the iBioID approach. The mechanism of reduced mIPSC frequency for InSyn1 is likely through the disruption of the ability of InSyn1 to form complexes with both gephyrin and the dystrophin complex at the iPSD. Loss of dystrophin might also lead to a secondary trans-synaptic effect on presynaptic release probability through its ability to bind neurexins (*22*, *23*).

Twenty-seven of the proteins of the iPSD, including several proteins first identified here, are implicated by either human or mouse genetics in seizure susceptibility and/or familial epilepsy, intellectual disability, or autism (Fig. 2G). Of the newly identified iPSD proteins implicated in developmental disorders, many are signaling proteins or are proteins of unknown functions (discussion in supplementary text). It is also interesting to note that 17 proteins overlapped between the inhibitory and excitatory PSD fractions. These could reflect dual synapses [spines containing gephyrin (*24*)] or might represent signaling proteins that transit between synapse types to facilitate synaptic crosstalk.

Our results indicate that the composition of the iPSD is far more complex than previously appreciated. This concept is in line both with emerging evidence of inhibitory synaptic plasticity at the postsynaptic specialization (*25*–*32*), and with our molecular evidence that the iPSD is associated with a variety of signaling proteins, analogous to that of excitatory synapses. The identification of the iPSD proteome provides a rational basis for investigating fundamental mechanisms that regulate synaptic inhibition. It also establishes a new reference frame to ascertain how perturbations of this protein complex may contribute to developmental brain disorders.

### REFERENCES AND NOTES


1. E. G. Gray, *J. Anat.* **93**, 420–433 (1959).
2. R. C. Malenka, M. F. Bear, *Neuron* **44**, 5–21 (2004).
3. M. B. Kennedy, H. C. Beale, H. J. Carlisle, L. R. Washburn, *Nat. Rev. Neurosci.* **6**, 423–434 (2005).
4. S. G. Grant, *Curr. Opin. Neurobiol.* **22**, 522–529 (2012).
5. L. Volk, S. L. Chiu, K. Sharma, R. L. Huganir, *Annu. Rev. Neurosci.* **38**, 127–149 (2015).
6. K. J. Roux, D. I. Kim, M. Raida, B. Burke, *J. Cell Biol.* **196**, 801–810 (2012).
7. D. I. Kim *et al.*, *Proc. Natl. Acad. Sci. U.S.A.* **111**, E2453–E2461 (2014).
8. Z. Yao, J. Petschnigg, R. Ketteler, I. Stagljar, *Nat. Chem. Biol.* **11**, 387–397 (2015).
9. A. Poulopoulos *et al.*, *Neuron* **63**, 628–642 (2009).
10. S. K. Tyagarajan, J. M. Fritschy, *Nat. Rev. Neurosci.* **15**, 141–156 (2014).
11. P. Prior *et al.*, *Neuron* **8**, 1161–1170 (1992).
12. J. W. Um *et al.*, *J. Biol. Chem.* **291**, 10119–10130 (2016).
13. Known iPSD proteins included eight $GABA_A$ receptor subunits, inhibitory transmembrane adhesion proteins [e.g., neuroligin-2 (*33*–*35*), Slitrk3 (*36*), and neuroplastin (*37*, *38*)], as well as signaling- and actin-associated proteins, such as Trim3 (*39*), Enah (*40*), profiling (*41*); and dystrophin complex proteins (including alpha-1-syntrophin, dystrobrevin alpha, and dystrophin) (*42*).
14. G. G. Gross *et al.*, *Neuron* **78**, 971–985 (2013).
15. S. Incontro, C. S. Asensio, R. H. Edwards, R. A. Nicoll, *Neuron* **83**, 1051–1057 (2014).
16. E. O. Mann, J. M. Suckling, N. Hajos, S. A. Greenfield, O. Paulsen, *Neuron* **45**, 105–117 (2005).
17. R. J. Platt *et al.*, *Cell* **159**, 440–455 (2014).
18. M. Pane *et al.*, *Neuromuscul. Disord.* **23**, 313–315 (2013).
19. E. A. Heller *et al.*, *PLOS ONE* **7**, e39572 (2012).
20. Y. Kang *et al.*, *J. Biol. Chem.* **289**, 29350–29364 (2014).
21. Y. Nakamura *et al.*, *J. Biol. Chem.* **291**, 12394–12407 (2016).
22. S. Sugita *et al.*, *J. Cell Biol.* **154**, 435–446 (2001).
23. D. E. Michele *et al.*, *Nature* **418**, 417–421 (2002).
24. K. L. Villa *et al.*, *Neuron* **89**, 756–769 (2016).
25. J. N. Bourne, K. M. Harris, *Hippocampus* **21**, 354–373 (2011).
26. I. Lushnikova, G. Skibo, D. Muller, I. Nikonenko, *Neuropharmacology* **60**, 757–764 (2011).
27. F. Niwa *et al.*, *PLOS ONE* **7**, e36148 (2012).
28. B. Dejanovic *et al.*, *PLOS Biol.* **12**, e1001908 (2014).
29. E. M. Petrini *et al.*, *Nat. Commun.* **5**, 3921 (2014).
30. C. E. Flores *et al.*, *Proc. Natl. Acad. Sci. U.S.A.* **112**, E65–E72 (2015).
31. J. L. Chen *et al.*, *Neuron* **74**, 361–373 (2012).
32. D. van Versendaal *et al.*, *Neuron* **74**, 374–383 (2012).
33. F. Varoqueaux, S. Jamain, N. Brose, *Eur. J. Cell Biol.* **83**, 449–456 (2004).
34. E. R. Graf, X. Zhang, S. X. Jin, M. W. Linhoff, A. M. Craig, *Cell* **119**, 1013–1026 (2004).
35. B. Chih, H. Engelman, P. Scheiffele, *Science* **307**, 1324–1328 (2005).
36. H. Takahashi *et al.*, *Nat. Neurosci.* **15**, 389–398, S1–S2 (2012).

37. P. W. Beesley, R. Herrera-Molina, K. H. Smalla, C. Seidenbecher, *J. Neurochem.* **131**, 268–283 (2014).
38. R. Herrera-Molina *et al.*, *J. Biol. Chem.* **289**, 8973–8988 (2014).
39. C. C. Cheung *et al.*, *Proc. Natl. Acad. Sci. U.S.A.* **107**, 11883–11888 (2010).
40. T. Giesemann *et al.*, *J. Neurosci.* **23**, 8330–8339 (2003).
41. K. Murk *et al.*, *PLOS ONE* **7**, e34167 (2012).
42. G. S. Pilgram, S. Potikanond, R. A. Baines, L. G. Fradkin, J. N. Noordermeer, *Mol. Neurobiol.* **41**, 1–21 (2010).

**ACKNOWLEDGMENTS**

This work was supported by NIH grants MH104736 (S.H.S.) and NS039444 (R.J.W.). We thank J. Ding for animal perfusions, B. Carlson for advice on image analysis, A. Swartz for cloning, and K. Sakurai and J. Takatoh for advice on AAV production and injection protocols. Raw data relating to all mass spectrometry–based experiments can be viewed or downloaded from www.ChorusProject.org under the project title "Uezu_Soderling_RawData_July2016."

**SUPPLEMENTARY MATERIALS**

www.sciencemag.org/content/353/6304/1123/suppl/DC1
Materials and Methods
Supplementary Text
Figs. S1 to S5
Tables S1 to S6
References (*43*–*61*)

6 May 2016; accepted 25 July 2016
10.1126/science.aag0821

VACCINES

# Protective efficacy of multiple vaccine platforms against Zika virus challenge in rhesus monkeys

**Peter Abbink,[1]* Rafael A. Larocca,[1]* Rafael A. De La Barrera,[2] Christine A. Bricault,[1] Edward T. Moseley,[1] Michael Boyd,[1] Marinela Kirilova,[1] Zhenfeng Li,[1] David Ng'ang'a,[1] Ovini Nanayakkara,[1] Ramya Nityanandam,[1] Noe B. Mercado,[1] Erica N. Borducchi,[1] Arshi Agarwal,[1] Amanda L. Brinkman,[1] Crystal Cabral,[1] Abishek Chandrashekar,[1] Patricia B. Giglio,[1] David Jetton,[1] Jessica Jimenez,[1] Benjamin C. Lee,[1] Shanell Mojta,[1] Katherine Molloy,[1] Mayuri Shetty,[1] George H. Neubauer,[1] Kathryn E. Stephenson,[1] Jean Pierre S. Peron,[3] Paolo M. de A. Zanotto,[3] Johnathan Misamore,[4] Brad Finneyfrock,[4] Mark G. Lewis,[4] Galit Alter,[5] Kayvon Modjarrad,[2,6] Richard G. Jarman,[2] Kenneth H. Eckels,[2] Nelson L. Michael,[2] Stephen J. Thomas,[2]† Dan H. Barouch[1,5]†‡**

**Zika virus (ZIKV) is responsible for a major ongoing epidemic in the Americas and has been causally associated with fetal microcephaly. The development of a safe and effective ZIKV vaccine is therefore an urgent global health priority. Here we demonstrate that three different vaccine platforms protect against ZIKV challenge in rhesus monkeys. A purified inactivated virus vaccine induced ZIKV-specific neutralizing antibodies and completely protected monkeys against ZIKV strains from both Brazil and Puerto Rico. Purified immunoglobulin from vaccinated monkeys also conferred passive protection in adoptive transfer studies. A plasmid DNA vaccine and a single-shot recombinant rhesus adenovirus serotype 52 vector vaccine, both expressing ZIKV premembrane and envelope, also elicited neutralizing antibodies and completely protected monkeys against ZIKV challenge. These data support the rapid clinical development of ZIKV vaccines for humans.**

The explosive and unprecedented ZIKV outbreak in the Americas (*1*, *2*) prompted the World Health Organization to declare this epidemic a public health emergency of international concern. ZIKV has been causally associated with fetal microcephaly, intrauterine growth retardation, and other congenital malformations in both humans (*3*–*6*) and mice (*7*–*9*), and it has also been linked with neurologic disorders such as Guillain-Barre syndrome (*10*). Several reports have shown that ZIKV can infect placental and fetal tissues, leading to prolonged viremia in pregnant women (*11*) and nonhuman primates (*12*). ZIKV also appears to target cortical neural progenitor cells (*7*–*9*, *13*, *14*), which likely contributes to neuropathology.

We recently reported the protective efficacy of two vaccines against ZIKV challenges in mice: a purified inactivated virus (PIV) vaccine from ZIKV strain PRVABC59 and a DNA vaccine expressing an optimized premembrane and envelope (prM-Env) immunogen from ZIKV strain BeH815744 (*15*). These studies used ZIKV challenge strains from Brazil (ZIKV-BR; Brazil/ZKV2015) (*9*) and Puerto Rico (ZIKV-PR; PRVABC59). ZIKV replication in mice was dependent on the mouse strain (*15*) and may be less extensive than in nonhuman primates (*12*). We therefore evaluated the immunogenicity and protective efficacy of inactivated virus, DNA-based, and vector-based vaccines against ZIKV challenge in rhesus monkeys.

## ZIKV PIV vaccine study

We first immunized 16 rhesus monkeys by the subcutaneous route with 5 μg of ZIKV PIV vaccine plus alum ($n$ = 8) or sham vaccine (alum only) ($n$ = 8) at weeks 0 and 4 (fig. S1). All PIV-vaccinated animals developed ZIKV Env–specific binding antibodies, as measured by enzyme-linked immunosorbent assays (ELISAs), and ZIKV-specific neutralizing antibodies, as measured by microneutralization (MN50) assays, at week 2 after initial immunization. Median log antibody titers at week 2 were 1.87 (Fig. 1A) and 2.27 (Fig. 1B) in ELISAs and MN50 assays, respectively. After the week 4 boost immunization, median log antibody titers increased substantially to 3.54 (Fig. 1A) and 3.66 (Fig. 1B), respectively, at week 6. In contrast, sham control monkeys did not develop detectable ZIKV-specific antibody responses (fig. S2). Binding antibody titers correlated with neutralizing antibody titers in the PIV-vaccinated animals ($P$ < 0.0001, coefficient of correlation $R$ = 0.88, Spearman rank correlation test; fig. S3). Only minimal antibody-dependent cellular phagocytosis responses were observed. The majority of PIV-vaccinated monkeys (Fig. 1, C and D), but not sham control animals (fig. S4), also developed modest cellular immune responses, primarily to Env, as measured by interferon (IFN)–γ enzyme-linked immunospot (ELISPOT) assays.

To assess the protective efficacy of the PIV vaccine against ZIKV challenge, we infected PIV-immunized and sham control monkeys by the subcutaneous route with $10^6$ viral particles [vp; $10^3$ plaque-forming units (PFU)] of ZIKV-BR or ZIKV-PR ($n$= 4 per group) (*15*). Viral loads after ZIKV challenge were quantitated by reverse transcription polymerase chain reaction (*15*), and viral infectivity was confirmed by growth in Vero cells. ZIKV-specific MN50 titers increased after challenge, particularly in the sham controls (fig. S5). Sham control monkeys exhibited 6 to 7 days of detectable viremia, with median peak viral loads of 5.82 log copies/ml (range, 5.21 to 6.29 log copies/ml; $n$ = 8) on day 3 to 5 after challenge (Fig. 2A). Virus was also detected in the majority of sham control animals in urine and cerebrospinal fluid (CSF) on day 3, as well as in colorectal secretions and cervicovaginal secretions on day 7 (Fig. 2, B to E). In contrast, PIV-vaccinated monkeys showed complete protection against ZIKV challenge, as evidenced by no detectable virus (<100 copies/ml) in the blood, urine, CSF, colorectal secretions, or cervicovaginal secretions in any animal after challenge ($n$ = 8; $P$ = 0.0002, Fisher's exact test comparing PIV-vaccinated animals with sham controls). We were unable to assess ZIKV in semen in the male animals in this study because of inadequate sample volumes. No major differences in plasma viral loads were observed between the sham controls that received ZIKV-BR versus those that received ZIKV-PR (fig. S6).

## Adoptive transfer studies

We next explored the mechanism of the observed protection through adoptive transfer studies.

[1]Center for Virology and Vaccine Research, Beth Israel Deaconess Medical Center, Harvard Medical School, Boston, MA 02215, USA. [2]Walter Reed Army Institute of Research, Silver Spring, MD 20910, USA. [3]University of São Paulo, São Paulo 05508-000, Brazil. [4]Bioqual, Rockville, MD 20852, USA. [5]Ragon Institute of MGH, MIT and Harvard, Cambridge, MA 02139, USA. [6]Henry M. Jackson Foundation, Bethesda, MD 20817, USA.
*These authors contributed equally to this work. †These authors contributed equally to this work. ‡**Corresponding author. Email: dbarouch@bidmc.harvard.edu**

# Identification of an elaborate complex mediating postsynaptic inhibition

Akiyoshi Uezu, Daniel J. Kanak, Tyler W. A. Bradshaw, Erik J. Soderblom, Christina M. Catavero, Alain C. Burette, Richard J. Weinberg and Scott H. Soderling

*Science* **353** (6304), 1123-1129.
DOI: 10.1126/science.aag0821